Digest Journal of Nanomaterials and Biostructures Vol. 19, No. 4, October-December 2024, p. 1547-1559

Structural and optical features improvement of Tm^{3+}–doped $B_2O_3 – BaSO_4 – TeO_2 – Na_2O$ glasses

S. Azmi [a], S. K. Ghoshal [a,b,*], F. Mohd-Noor[a], S. A. Jupri [a], A. S. Alqarni [c]
[a] *Physics Department (AOMRG), Faculty of Science, Universiti Teknologi Malaysia (UTM), Johor Bahru, Johor, Malaysia*
[b] *Snano (ISI-SIR), Laser Center & Physics Department (AOMRG), Faculty of Science, Universiti Teknologi Malaysia (UTM), Johor Bahru, Johor, Malaysia*
[c] *Department of Physics, College of Science, Princess Nourah binti Abdulrahman University, P.O. Box 84428, Riyadh 11671, Saudi Arabia*

Highly transparent sodium-telluro-sulphate-borate glasses doped with thulium (Tm^{3+}) were useful for variety of purposes. Thus, a new type of glass system composed of (57-x)B_2O_3 – 20$BaSO_4$ – 13TeO_2 – 10Na_2O – (x)Tm_2O_3 (x = 0.2 to 0.8 mol%) was produced via standard melt-quenching route. The impacts of different Tm^{3+} contents on the glasses' physical and optical characteristics were ascertained for the first time. The amorphous nature of the samples was validated by their XRD patterns, and Raman analysis revealed the presence of various chemical functional groups. These samples exhibited Urbach energy, direct band gap and indirect band gap between 0.088 – 0.262 eV, 2.458 – 2.545 eV and 2.098 – 2.425 eV respectively. UV-Vis-NIR absorbance displayed six prominent peaks at 464, 657, 686, 795, 1210 and 1680 nm characteristics to various electronic transitions of Tm^{3+}. The prepared glass composition could be effective in the production of solid-state lasers with a narrow wavelength range.

(Received August 7, 2024; Accepted October 18, 2024)

Keywords: Thulium oxide (Tm_2O_3), Structural properties, Optical bandgap, Borate glass

1. Introduction

Numerous studies have been conducted to prepare better material for solid-state lasers targeted to the LEDs fabrication. Transparent materials like glasses are more desirable for illumination devices making than other materials due to their many interesting properties. Different types of glass hosts including phosphate, tellurite, borate, and silicate, have been prepared and characterized for various reasons [1-4]. Few distinctive traits such as easy synthesis, high thermal and chemical stability, low melting temperature, excellent transparency, cost effectiveness, and appropriate solubility for diverse elements make borate the material of choice for various purposes despite their hygroscopic features [5-7]. Therefore, to resolve this problem, some of the studies have been performed by adding several elements to the borate hosts such as sodium, tellurite and barium [8,9]. The improvements accomplished due to such inclusion enable the borate-based glass system highly desirable glass formers for varied practical uses [10,11].

Previous literature [12] reported that adding rare earth elements to glass systems is vital for improving glass quality. Rare earth ions have the ability to affect the structure and characteristics of multiple component glass compositions in addition to acting as an optically active agent [13]. Moreover, the stabilization and resistance to crystallization of glass are improved by the addition of rare earth elements [14]. The Tm^{3+} ion ($4f^{12}$) is deemed a notable ion among rare-earth ions because it has two meta-stable excited levels of $^1D_2$ and $^1G_4$ in its energy-level structure, allowing it to emit blue light either normally or through NIR up-conversion [15,16]. Furthermore, it was discovered that the addition of Tm^{3+} greatly lowers the glass

* Corresponding author: sibkrishna@utm.my
https://doi.org/10.15251/DJNB.2024.194.1547

refractive index. It was also surmised that Tm^{3+} can occupy the glass network positions, thus altering the oxides arrangements and stabilizing the NBO linkages [17]. Based on these qualities of Tm^{3+} for strong illumination applications it became viable for other uses such as visible laser, optical fiber amplifiers, atmospheric pollution monitoring, medical procedures, satellite imaging and safe-vision laser radar [18-22].

Presently, the purpose of this work is to improve the structural and optical characteristics of B_2O_3 – $BaSO_4$ – TeO_2 – Na_2O glasses made using the melt-quenching approach by incorporating thulium oxide (Tm_2O_3) into the glass system. The concentration of thulium oxide was varied to determine its effect on various characteristics of the glasses. The measured UV- Vis, physical and structural of the samples were evaluated to confirm their validity. The results revealed that the suggested glass composition has a lot of potential for developing narrow-range solid-state lasers.

2. Experimental details

2.1. Sample preparation

The current glass samples with a composition of $(57\text{-}x)B_2O_3$ – $20BaSO_4$ – $13TeO_2$ – $10Na_2O$ – $(x)Tm_2O_3$; x = 0.2 – 0.8 mol% were synthesized by utilizing the conventional melt-quenching procedure. The high purity of 99.0% raw material such as thulium oxide (Tm_3O_3), sodium oxide (Na_2O), tellurium dioxide (TeO_2), barium sulphate ($BaSO_4$) and boric acid (H_3BO_3) were utilized to make the proposed glasses. Then, for each sample, all the ingredients (~10 g) of specific proportions were mixed uniformly and milled for about 1 hour (Table 1). Subsequently, every mixture was placed inside an alumina crucible, which was then melted at 1300 °C for an hour in an electrical furnace. The melting mixture was then poured on a pre-heated stainless- steel plate for 3 hours at 400 °C to avoid embrittlement and release the stress. The samples were then polished for optical studies. Depending on the amount of Tm_2O_3 (mol%) these glass samples were labeled as BSTNTm0.2, BSTNTm0.4, BSTNTm0.6 and BSTNTm0.8.

Table 1. Name, nominal composition, and physical appearance of the studied glass system.

Glass code	Composition (mol%)					Physical Appearance
	B_2O_3	$BaSO_4$	TeO_2	Na_2O_3	Tm_2O_3	
BSTNTm0.2	56.8	20	13	10	0.2	Transparent, colorless, non-hygroscopic
BSTNTm0.4	56.6	20	13	10	0.4	Transparent, colorless, non-hygroscopic
BSTNTm0.6	56.4	20	13	10	0.6	Transparent, colorless, non-hygroscopic
BSTNTm0.8	56.2	20	13	10	0.8	Transparent, colorless, non-hygroscopic

2.2. Sample characterization

Several analytical instruments were used to analyze all the studied samples at ambient temperature. The amorphous nature of the Tm^{3+}-doped BSTN samples (ground in fine powder form) was verified using Rigaku X-Ray Diffractometer. The XRD peaks of samples were recorded at 2θ range between 10 to 100°. The Archimedes method was employed to determine the densities of the glasses, with distilled water serving as the immersion liquid. The bulk glass density was measured by Mettler Toledo density meter. The value of glass density (ρ_s) was calculated using:

$$\rho_s = \frac{W_a}{W_a - W_b}\rho_o \quad (1)$$

where ρ_o is distilled water density ($\rho_o = 1\ g/cm^3$). W_a and W_b are the weight of glass in air and in distilled water respectively. The formation of free excess volume based on the size of gaps within the glass structure during glass modification were represented as molar volume (V_m) [23]. The value of V_m was obtained via:

$$V_m = \frac{M_w}{\rho_s} \tag{2}$$

where M_w is the molecular weight. Other physical characteristics such as Tm^{3+} concentration (N_i), polaron radius (r_p), interionic separation (r_i) and strength of field around Tm^{3+} in the glass matrix (F) was evaluated via [8]:

$$N_i = \frac{N_A\, \rho_S\, X}{M_{av}} \tag{3}$$

$$r_p(\text{Å}) = \frac{1}{2}\left(\frac{\pi}{6N_i}\right)^{1/3} \tag{4}$$

where N_A, X and M_{av} denote the Avogadro number, mole fraction of dopant and sample molecular weight, respectively. Additional parameters that are related to the value of ion concentration is as below:

$$F = \frac{Z}{{r_p}^2} \tag{5}$$

$$r_i = \left(\frac{1}{N_i}\right)^2 \tag{6}$$

where F is field strength, dopant atomic number, Z and r_i is the inter-nuclear distance.

Raman spectra from 200 to 1400 cm^{-1} were acquired using the HORIBA Scientific Raman LABRam HR Evolution spectrophotometer. The samples' UV-Vis optical absorption was obtained between 200–1600 nm and recorded using Shimadzu Model 86000 Plus UV-Vis NIR Spectrophotometer. The samples' absorption coefficient (α) were evaluated from absorption spectra using [24]:

$$\alpha = 2.303\ \frac{A}{d} \tag{7}$$

where A and d are the corresponding sample's absorbance and thicknesses (in cm). Mott–Davis equation was utilized to calculate the glasses optical band gap energy (E_{opt}) values based on the incident photon energy (hv):

$$\alpha = \frac{B\left(hv - E_{opt}\right)^r}{hv} \tag{8}$$

where the band tailing constant, denoted by parameter B, while the nature of band-to-band electronic absorption transitions, indicated by parameter r ($r = 1/2$ and $r = 2$ are the corresponding indirect and direct allowed transition) [25]. The samples' Urbach energy (ΔE) values were computed from the slope reciprocal of ln α versus hv plots via:

$$\alpha = \alpha_o\ exp\left(\frac{hv}{\Delta E}\right) \tag{9}$$

where α_o is a constant (intercept). The values of molar polarization (α_m), molar refraction (R_m) and refractive index (n) of the glasses were obtained via [26]:

$$\frac{(n^2-1)}{(n^2+2)} = 1 - (\frac{E_{opt}}{20})^{1/2} \quad (10)$$

$$R_m = \frac{(n^2-1)}{(n^2+2)} V_m \quad (11)$$

$$\alpha_m = (\frac{3}{4}\pi N_A) R_m \quad (12)$$

where $\alpha_m = R_m/2.52$, ε is the dielectric constant ($\varepsilon = n^2$), R symbolize glass surface reflection loss ($R = (n-1/n+1)^2$) while £ represent optical dielectric constant ($£ = n^2 - 1$) [3]. Every optical analysis was conducted on properly polished bulk samples with a smooth and transparent parallel surface to reduce signal noise and a better absorption spectrum.

3. Results and discussion

3.1. Amorphous phase and density of glasses

Fig 1 shows the XRD pattern of the selected samples which showed their amorphous character due to the existence of diffuse broad halo and without any sharp peak, suggesting no crystallization in the sample [27]. Besides, the prepared samples displayed a variety of broad characteristics that suggested structural heterogeneity in addition to just one typical amorphous halo [28].

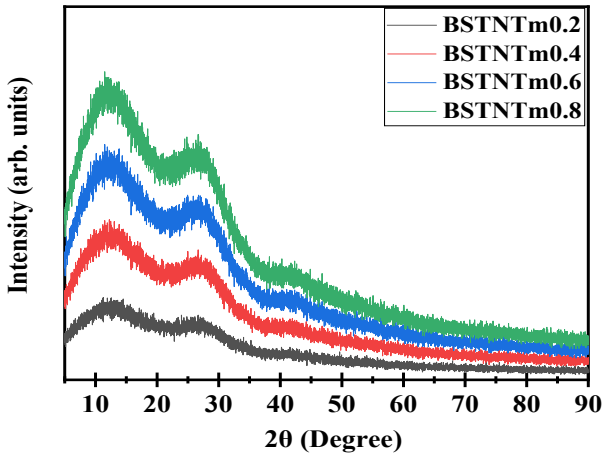

Fig. 1. XRD glasses profiles.

Table 2 shows the impact of Tm^{3+} contents dependent glass densities and molar volumes. Figure 2 illustrates variations in density and molar volume at different Tm^{3+} concentrations. The glass density rose with Tm^{3+} doping to 0.6 mol% and thereafter marginally decreased. In contrast, the molar volume significantly decreased up 0.6 mol% Tm^{3+} and somewhat increased with a further addition of Tm^{3+}. The density results showed anomalies pattern which was elevated and at a certain point reduced. The density was inversely related to the glass molar volume. The increase in density with the inclusion of Tm^{3+} up to 0.6 mol% (Fig. 2.) was mainly because of the dopant greater molecular weight than other host materials [29]. The inclusion of Tm^{3+} to the glass network increases the glass's total molecular weight since density is directly proportional to the mass, hence its results in the increasing of density [30]. Also, the lower ionic radii of Tm^{3+} allowed them to fill the interstitial regions within the host matrix, resulting in compact glass [26]. Oppositely, with the further addition of Tm^{3+} up to 0.8 mol%, the non-bridging oxygen increased so the density slightly decreased due to an increase in oxygen packing which squeezes the structure of the sample. Conversely, the shrinking of bond lengths or the interatomic distance between the atoms that constitute the network may be the cause of the molar volume value dropping from 34.82 to 34.34 cm^3 mol^{-1}, which would cause the glass network structure to become compacted [31].

The other physical properties of the BSTN glass system doped with rare earth (Tm^{3+}) were calculated from the equation (3) to (6) from section 2.2 and recorded in Table 2. The polaron radius decreased as the quantity of Tm^{3+} ions in the glass increased from $2.66 \times 10^{-8} - 1.68 \times 10^{-8}$ Å. The numbers indicate that the polaron is low, as they do not exceed the lattice constants of the various oxides in the glass [32,33]. Besides, a gain in glass compactness and polarizability was correlated with the polaron radius declining which resulted in increasing in the glass electrical conductivity [34,35].

Table 2. Physical parameters of Tm^{3+} doped sodium-telluro-barium sulphur-borate glass system.

Physical parameters	Glass code			
	BSTNTm0.2	BSTNTm0.4	BSTNTm0.6	BSTNTm0.8
Average molecular weight, Mw_{av} (g)	113.94	114.57	115.20	115.84
Density, ρ (g/cm^3)	3.27	3.31	3.36	3.32
Molar volume, V_m (cm^3/mol)	34.82	34.60	34.34	34.86
RE ion concentration, N_i (ions/cm^3)	3.46×10^{21}	6.96×10^{21}	1.05×10^{22}	1.38×10^{22}
Poloron radius, r_p (10^{-8} Å)	2.66	2.11	1.84	1.68
Inter ionic separation, r_i (10^{-8} Å)	6.61	5.24	4.56	4.17
Field strength, F (cm^{-2})	9.72×10^{16}	1.55×10^{17}	2.04×10^{17}	2.45×10^{17}

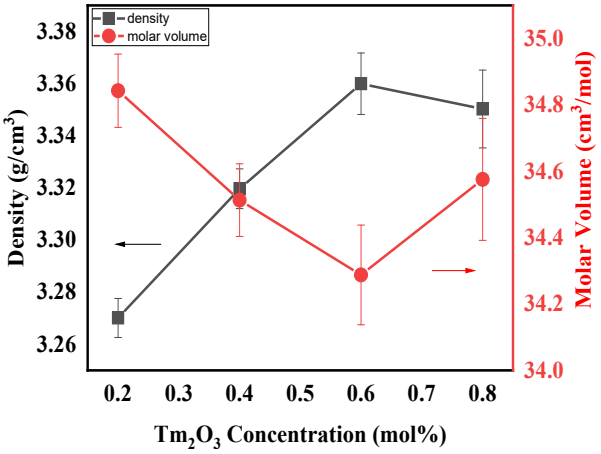

Fig. 2. Glass density and molar volume against Tm_2O_3 concentration.

3.2. Raman spectral analysis of glasses

Fig. 3 depicts the typical Raman lines of samples ranging from 300 – 1500 cm^{-1}. As illustrated in Fig. 4, the spectrum is deconvoluted into seven peaks, which are referred to as peak A, B, C, D, E, F, and G. Table 3 lists the observed spectral peak position and their corresponding band assignments. The 355 – 367 cm^{-1} band (peak A) are caused due to the interactions between NBO and network structural unit of TeO_3 trigonal pyramid (tp) [36]. The IR absorption band of peak B (464 – 468 cm^{-1}) was caused by the bending vibration modes of TeO_4 units associated with Te – O – Te and O – Te – O interactions [36, 37]. The vibration of the sulphate (SO_4) groups induced the peak of the Raman at 540 – 563 cm^{-1} (peak C), which is compatible with literature reported by [38]. Around 500 – 600 cm^{-1} the bending modes of (SO_4) and (BO_4) are observed. The spectra between 400 – 1000 cm^{-1} are dominated by the modes of the bridging S – O and B – O bonds, which is agrees with the data of the studies for SO_4 and BO_4 tetrahedra [39,40]. The massive band detected as peak D (768 cm^{-1}) was produced by the combination of Te – O vibrations modes associated with TeO_3 tp units and symmetric breathing vibration modes of 6-coordinated rings and the substitution of the BO_3 triangle by the BO_4 tetrahedra [36]. The band

detected between 984 – 987 cm^{-1} is a result of the stretching of tetrahedral B – O bonds [BO_4] [41]. The IR absorption band around 1039 – 1041 cm^{-1} was primarily driven by the existence of pentaborate network units within the borate matrix [36]. The triangles connected with additional units of triangular borate groups (BO_3) was the reason for the band detected between 1336 - 1347 cm^{-1} [42]. Overall, there is not much difference in intensity with the addition of Tm^{3+} ions due to the small amount of dopant which is less than 1.0 mol%. However, the elongation of O – Te – O bond is shown by the peak's slight shift down to lower wavenumber, resulting in more symmetrical structure in the glass. The optimum phonon energy of the glass former, as revealed by the Raman spectra, is 768 cm^{-1}, which is comparatively less than the values seen in silicate (889 cm^{-1}) [43] and phosphate (1120 cm^{-1}) [44] glass systems.

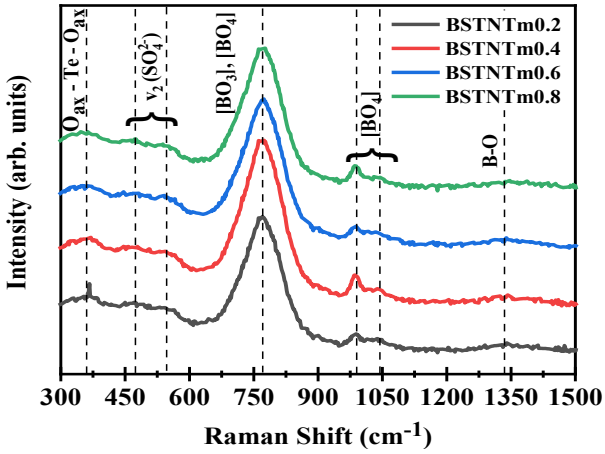

Fig. 3. Raman spectra of synthesized glasses.

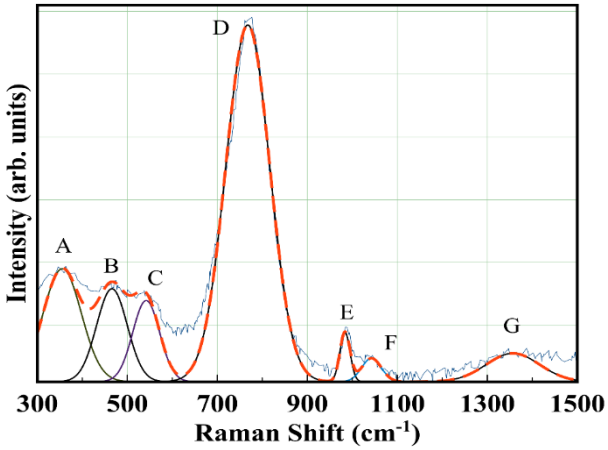

Fig. 4. Deconvulated Raman spectra of BSTNTm0.8 glass.

Table 3. Comparison of Raman bands assignment and their position for the present glasses with previously documented glass system.

Glass Code				Reported	Assignment
BSTNTm0.2	BSTNTm0.4	BSTNTm0.6	BSTNTm0.8		
367	363	358	355	363 [45] 371 [46]	Axial bonding vibrational mode (Oax – Te – Oax)
468	466	464	466	405 – 460 [47-50]	The bending vibrations of TeO_4
563	558	540	542	460 [36], [37] 544 [51] 500 – 600 [38]	Doubly generated symmetric bending modes V_2 (SO_{2-}^{4}) / modes of sulphate groups (SO_{2-}^{4})
768	768	768	768	774 – 793 [52] 765 [53] 710 – 810 [54] 773 [55]	Six-membered-ring's breathing vibration with $[BO_3]$ triangle $[BO_4]$
986	987	986	984	953 – 1103 [56]	Tetraborate, pyroborate, orthoborate, and diborate groups respectively
1039	1039	1041	1043		
1346	1343	1346	1347	1308 – 1328 [51],[57] 1300 – 1600 [56]	B – O band asymmetric stretching vibration in the BO_3 group B – O metaborate rings stretching

3.3. Optical absorption spectra of glasses

Fig. 5 displays the UV-Vis absorption spectra of Tm^{3+} in BSTN glass ranges from 400 to 2000 nm with composition (57-x)B_2O_3 – 20$BaSO_4$ – 13TeO_2 – 10Na_2O – (x)Tm_2O_3; at ambient temperature; x = 0.2 to 0.8 mol. For Tm^{3+} -doped sodium telluro sulphate borate glass, every form and peak locations are clearly comparable to those present in different Tm^{3+} -doped glasses [2,17,58, 59-60]. The absorption spectrum involves six absorption band peaks at around 1680, 1210, 795, 686, 657 and 464 respectively. This is because, in the excitation states ($^3F_4$, $^3H_5$, $^3H_4$, $^3F_3$, $^3F_2$ and $^1G_4$), Tm^{3+} ground state ($^3H_6$) is absorbed. Regarding the pattern observed in Fig. 6., there are no alteration to the absorption peaks' wavelength as the concentration of Tm^{3+} doped BSTN increases, however the absorption intensity is directly correlated with the Tm^{3+} concentration showing that the Tm^{3+} ions have integrated uniformly into the glassy matrix with no clustering or modifications to the local ligand field [17].

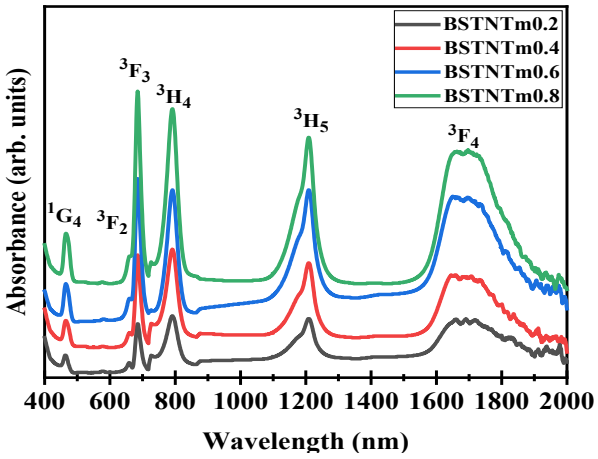

Fig. 5. The glasses' optical absorption spectrum.

Figs. 6, 7 and 8 depict the Tauc plots for the glass system. The variation of optical variables for Tm^{3+} doped BSTN glass including refractive index, molar refractivity, electron polarization and optical band gap was depicted in Table 4. Both indirect (2.098 – 2.425 eV) and direct (2.458 – 2.544 eV) optical band gap values of the glasses were increased due to the inclusion of thulium oxide; these values are slightly lower (2.7 eV) compared to the previous study [61]. This discrepancy may arise from the glass network' BO and NBO figures changing. Ultimately, the optical band gap expanded, and the glass polarizability plummeted as the NBO numbers decreased. Generally, electrons from the NBO can be excited more easily compared to BOs, making BOs less polarizable than NBOs. The E_{opt} values' increment may be attributed to Tm^{3+} doping enhancing the glass network' connection [26]. According to Azlan [62], Urbach energy delivers information regarding flaws and abnormalities existing within the glass structure. In this assessment, the Urbach energy shows a decrement with the addition of Tm^{3+} which lies within 0.262 – 0.088 eV. The decrease in defects in the composition of the glass is reflected in the decline of Urbach energy. Moreover, proved that the glass was very stable, especially the sample with 0.8 mol% Tm_2O_3 which has the lowest Urbach energy's number. In addition, the structural units of BO_4 and TeO_4 were mutually linked by forming stronger $BTeO_3$ and $BTeO_5$ units thereby minimizing the defects within the glass lattice [26]. Molar refractivity and polarizability were closely correlated with refractive index. Each of these parameters showed the same trend, which was opposed to the energy band gap, based on the value stated in Table 4. All these three variables generally declined as the amount of Tm^{3+} in the glass increased. The molar polarizability change was a crucial influence on the refractive index variation wherein cations strongly influenced the polarizability and BO number inside glass structure. The refractive index and molar refraction' decrement might be due to generation of more BO (weakly polarizable compared to NBO), yielding a decrease in the molar polarizability [26].

Based on the findings in structural and optical characterization, the presence of thulium oxide at higher concentration likely led to the probability formation of Te – O – Tm where thulium oxide acts as the network modifier, contributing to increased symmetry within the glass structure.

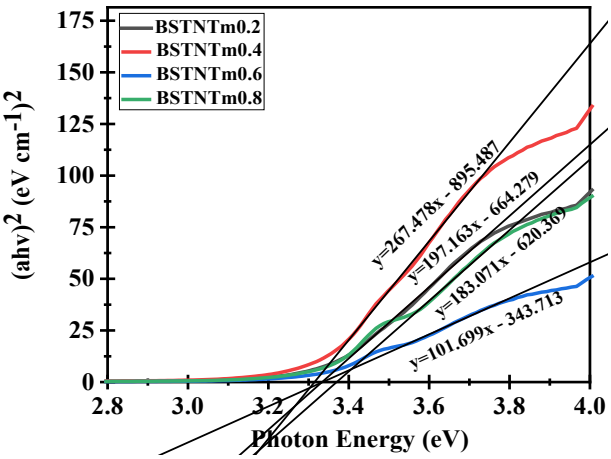

Fig. 6. Tauc's plot of the glasses for direct optical transitions.

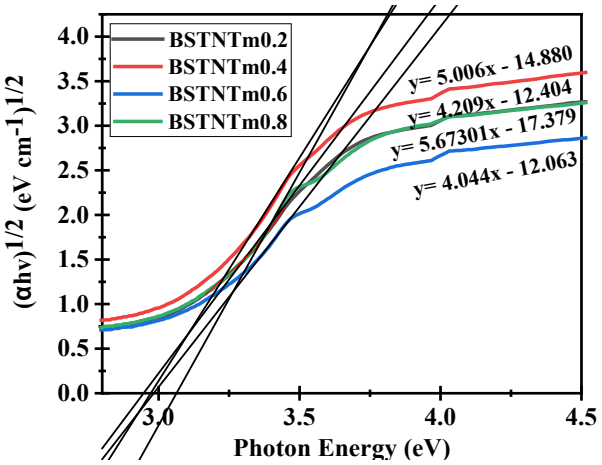

Fig. 7. Tauc's plot of the glasses for indirect optical transitions.

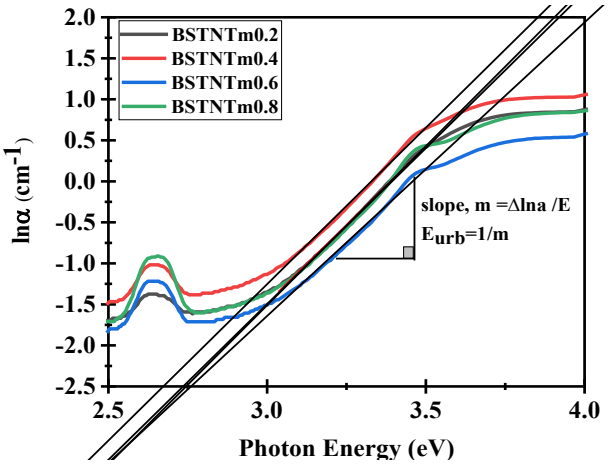

Fig. 8. Urbach plot of the glasses.

Table 4. Tm^{3+} -doped BSTN glasses' optical parameters.

Optical parameters	Glass code			
	BSTNTm0.2	BSTNTm0.4	BSTNTm0.6	BSTNTm0.8
Refractive index, n	2.412	2.405	2.402	2.380
Dielectric constant, ε	5.816	5.782	5.768	5.665
Optical dielectric constant, £	4.816	4.782	4.768	4.665
Reflection losses, R	0.171	0.170	0.169	0.167
Molar refractivity (cm^3/mol)	21.468	21.208	21.046	21.044
Electron polarizability (Å)	8.519	8.416	8.352	8.351
Direct bandgap (eV)	3.369	3.348	3.380	3.389
Indirect bandgap (eV)	2.947	2.972	2.983	3.063
Urbach energy (eV)	0.243	0.240	0.237	0.221

4. Conclusion

The influence of Tm_2O_3 activation at various contents (x = 0.2 - 0.8 mol%) on the optical, structural and physical characteristics of $(57\text{-}x)B_2O_3 - 20BaSO_4 - 13TeO_2 - 10Na_2O - (x)Tm_2O_3$ glasses was assessed for the first time. The glass amorphous state was verified by XRD test. It was found that raising the Tm_2O_3 content in place of B_2O_3 by increasing the optical band gap energy and density of the glasses while decreasing their refractive index, molar volume and Urbach energy (minimal defects). The symmetric breathing modes of six-member ring with the BO_4 tetrahedra replacing the BO_3 triangle and the vibration of Te – O from TeO_3 tp units were discovered as Raman band at 768 cm^{-1} which was caused by the conversion of BO to NBO in the glass matrix. It is affirmed that the proposed glass composition with excellent structural and optical features is beneficial for building narrow range solid-state lasers.

Acknowledgements

This study is funded by Universiti Teknologi Malaysia (UTM) under grant number UTMFR (21H78). Authors are grateful to the Ministry of Higher Education and UTM Zamalah scholarship. Also, we are grateful for the experimental support provided by Universiti Teknologi Malaysia's Faculty of Science and University Industry Research Laboratory (UIRL), PPMU.

References

[1] T. K. Seshagiri, N. K. Porwal, V. Sudersan, T. K. Gundu Rao, A. K. Tyagi, S. V. Godbole, Journal of Non-Crystalline Solids, 356, 1032 (2010); https://doi.org/10.1016/j.jnoncrysol.2010.01.019

[2] H. Gebavi, D. Milanese, R. Balda, M. Ivanda, F. Auzel, J. Lousteau, J. Fernandez, M. Ferraris, Optical Materials, 33, 428 (2011); https://doi.org/10.1016/j.optmat.2010.10.013

[3] Y. A. Yamusa, Rosli Hussin, W. N. Wan Shamsuri, Y. A. Tanko, Siti Aisha Jupri, Optik, 164, 324 (2018); https://doi.org/10.1016/j.ijleo.2018.03.019

[4] D. Porosz, J. Zmojda, M. Kochanowicz, P. Miluski, P. Jelen, M. Sitarz, Spectrochima Acta Part A: Molecular and Biomolecular Spectroscopy, 134, 608 (2015); https://doi.org/10.1016/j.saa.2014.06.070

[5] K. M. Kaky, M. I. Sayyid, A. Khammas, Ashok Kumar, Erdem Sakar, A. H. Abdalsalam, Betül Ceviz Şakar, Bünyamin Alim, M. H. A. Mhareb, Materials Chemistry and Physics, 242, 122504 (2020); https://doi.org/10.1016/j.matchemphys.2019.122504

[6] Y. S. M. Alajerami, S. Hashim, S. K. Ghoshal, D. A. Bradley, M. Mhreb, M. A. Saleh,

Journal of Luminescence, 155, 141-148 (2014); https://doi.org/10.1016/j.jlumin.2014.06.013

[7] S. Hashim, M. H. A. Mhreb, S. K. Ghoshal, Y. S. M. Alajerami, D. A. Bradley, M. I. Saripan, M. Tamchek, K. Alzimami, Radiation Physics and Chemistry, 116, 138-141 (2015); https://doi.org/10.1016/j.radphyschem.2015.04.007

[8] M. H. A. Mhareb, Muna Alqahtani, Fatimh Alshahri, Y. S. M. Alajerami, Noha Saleh, N. Alonizan, M. I. Sayyed, M. G. B. Ashiq, Taher Ghrib, Sarah Ibrahim Al-Dhafar, Tasneem Alayed, Mohamed A. Morsy, Journal of Non-Crystalline Solids, 541, 120090 (2020); https://doi.org/10.1016/j.jnoncrysol.2020.120090

[9] L. Bingrui, L. Desheng, Edwin Yue Bun Pun, Hai Lin, Journal of Luminescence, 206, 70 (2019); https://doi.org/10.1016/j.jlumin.2018.10.016

[10] Vinod Hegde, Naveen Chauhan, V. C. Petwal, Vijay Pal Verma, Jishnu Dwivedi, K. K. Mahato, Sudha D. Kamath, Nuclear Instruments and Methods in Physics Research Section B, 446, 5 (2019); https://doi.org/10.1016/j.nimb.2019.03.020

[11] S. Hashim, S. K. Ghoshal, I. Abdullahi, Indian Journal of Physics, 94, 1811 (2019); https://doi.org/10.1007/s12648-019-01631-3

[12] I. V. Kityk, J. Wasylak, S. Benet, D. Dorosz, J. Kucharski, J. Krasowski, B. Sahraoui, Journal of Applied Physics, 92, 2260 (2002); https://doi.org/10.1063/1.1498888

[13] M. N. Ami Hazlin, M. K. Halimah, F. D. Muhammad, Journal of Luminescence, 196, 498 (2018); https://doi.org/10.1016/j.jlumin.2017.11.054

[14] W. A. Pisarski, T. Goryczka, B. Wodecka-Duś, M. Płońska, J. Pisarska, Material Science and Engineering: B, 122, 94 (2005); https://doi.org/10.1016/j.mseb.2005.05.002

[15] G. Poirier, F. C. Cassanjes, C. B. Araujo, V. A. Jerez, S. J. L. Ribeiro, Y. Messaddeq, M. Poulain, Journal of Applied Physics, 93, 3259 (2003); https://doi.org/10.1063/1.1555674

[16] H. Lai, B. Chen, W. Xu, X. Wang, Y. Yang, Q. Meng, Journal of Alloys and Compounds, 395, 181 (2005); https://doi.org/10.1016/j.jallcom.2004.10.074

[17] Y. Tian, R. Xu, L. Zhang, L. Hu, J. Zhang, Journal of Applied Physics, 108, 083504 (2010); https://doi.org/10.1063/1.3499283

[18] D. H. Cho, Y. G. Choi, K. H. Kim, Chemical Physics Letter, 322, 263 (2000); https://doi.org/10.1016/S0009-2614(00)00408-5

[19] F. Cornacchia, A. Toncelli, M. Tonelli, Progress in Quantum Electronics, 33, 61(2009); https://doi.org/10.1016/j.pquantelec.2009.04.001

[20] S. D. Jackson, S. Mossman, Applied Physics B: Lasers and Optics, 77, 489 (2003); https://doi.org/10.1007/s00340-003-1305-5

[21] Y. Tsang, A. El-Tahxer, T. King, K. Chang, and S. Jackson, Optics Letter, 29, 334 (2006).

[22] D. F. de Sousa, L. F. C. Zonetti, M. J. V. Bell, J. A. Sampaio, L. A. O. Nunes, M. L. Baesso, A. C. Bento, L. C. M. Miranda, Applied Physics Letter, 74, 908 (1999); https://doi.org/10.1063/1.123406

[23] A. M. Sanad, A. G. Moustafa, F. A. Moustafa and A. A. El-Mongy, Central Glass and Ceramic Research Institute Bulletin, 32 53 (1985).

[24] V. C. V. Gowda, K. R. S. Pasha, M. S. Reddy, C. N. Reddy, Advance Materials Research, 584, 207 (2012); https://doi.org/10.4028/www.scientific.net/AMR.584.207

[25] M. Seshadri, E. F. Chillcce, J. D. Marconi, F. A. Sigoli, Y. C. Ratnakaram, L. C. Barbosa, Journal of Non-Crystalline Solids, 402, 141 (2014); https://doi.org/10.1016/j.jnoncrysol.2014.05.024

[26] L. Hasnimulyati, M. K. Halimah, A. Zakaria, S. A. Halim, M. Isshak, C. Eevon, Journal of Ovonic Research, 12, 291 (2016).

[27] Le-qi Yao, Guo-hua Chen, San-chuan Cui, Hai-ji Zhong, Cun Wen, Journal of Non-Crystallibe Solids, 444, 38 (2016); https://doi.org/10.1016/j.jnoncrysol.2016.04.039

[28] Z. Y. Yao, D. Möncke, E.I. Kamitsos, P. Houizot, F.Célarié, T. Rouxel, L. Wondraczek, Journal of Non-Crystalline Solids, 435, 55 (2016); https://doi.org/10.1016/j.jnoncrysol.2015.12.005

[29] N. Baizura, A. K. Yahya, Journal of Non-Crystalline Solids, 357, 2810 (2011); https://doi.org/10.1016/j.jnoncrysol.2011.03.003

[30] M. Khanisanij and H. A. A. Sidek, Advance in Materials Science and Engineering, 8 pages (2014); https://doi.org/10.1155/2014/452830

[31] T. G. V. M. Rao, A. Rupesh Kumar, K. Neeraja, N. Veeraiah, M. Rami Reddy, Spectrochima. Acta Part A: Molecular and Biomolecular Spectroscopy, 118, 744 (2014); https://doi.org/10.1016/j.saa.2013.09.061

[32] S. J. F. Byrnes, Basic theory and phenomenology of polarons, University of California, Barkley, 6 pages (2008).

[33] P. P. Pawar, S. R. Munishwar, S. Gautam, R. S. Gedam, Journal of Luminescence, 183, 79 (2017); https://doi.org/10.1016/j.jlumin.2016.11.027

[34] V. Thakur, A. Singh, R. Punia, S. Dahiya, L. Singh, Journal of Alloys and Compound, 696, 529 (2017); https://doi.org/10.1016/j.jallcom.2016.11.230

[35] L. D. Landau, S. I. Pekar, Ukrainian Journal of Physics, 423, 71 (1948).

[36] P. Suthanthirakumar, C. H. Basavapoornima, K. Marimuthu, Journal of Luminescence, 187, 392 (2017); https://doi.org/10.1016/j.jlumin.2017.03.052

[37] S. O. Baki, L. S. Tan, C. S. Kan, H. M. Kamari, A. S. M. Noor, M. A. Mahdi, Journal of Non-Crystalline solids, 362, 156 (2013); https://doi.org/10.1016/j.jnoncrysol.2012.11.042

[38] M. Daub, K. Kazmierczak, P. Gross, H. Höppe, H. Hillebrecht, Inorganic Chemistry, 52, 6011 (2013); https://doi.org/10.1021/ic400267s

[39] L. Jun, X. Shuping, G. Shiyang, Spectrochima. Acta Part A: Molecular and Biomolecular Spectroscopy, 51, 519 (1995); https://doi.org/10.1016/0584-8539(94)00183-C

[40] J. T. Kloprogge, H. Ruan, L. V. Duong, R. L. Frost, Netherlands Journal of Geoscience, 80, 41 (2001); https://doi.org/10.1017/S0016774600022307

[41] G. Rama Sundari, V. Pushpa Manjari, T. Raghavendra Rao, D. V. Satish, Ch. Rama Krishna, Ch. Venkata Reddy, R. V. S. S. N. Ravikumar, Optical Materials, 36, 1329 (2014); https://doi.org/10.1016/j.optmat.2014.03.023

[42] P. Damas, J. Coelho, G. Hungerford, N. S. Hussein, Materials Research Bulletin, 47, 3489 (2012); https://doi.org/10.1016/j.materresbull.2012.06.071

[43] M. Murali Mohan, L. Rama Moorthy, D. Ramachari, C. K. Jayasankar, Spectrochima Acta Part A: Molecular and Biomolecular Spectroscopy, 118, 966 (2014); https://doi.org/10.1016/j.saa.2013.09.094

[44] C. R. Kesavulu, K. Kiran Kumar, N. Vijaya, Ki-Soo Lim, C. K. Jayasankar, Materials Chemistry and Physics, 141, 903 (2013); https://doi.org/10.1016/j.matchemphys.2013.06.021

[45] K. Damak, El Sayed Yousef, A. S. Al-Shihri, H. J. Seo, C. Rüssel, R. Maâlej, Solid State Science, 28, 74 (2014); https://doi.org/10.1016/j.solidstatesciences.2013.12.012

[46] P. Karthikeyan, P. Suthanthirakumar, R. Vijayakumar, K. Marimuthu, Journal of Molecular Structure, 1083, 268 (2015); https://doi.org/10.1016/j.molstruc.2014.12.003

[47] S. A. Jupri, S. K. Ghoshal, M. F. Omar, N. N. Yusof, Journal of Alloys Compound, 753, 446 (2018); https://doi.org/10.1016/j.jallcom.2018.04.218

[48] A. Thieme, D. Möncke, R. Limbach, S. Fuhrmann, E.I. Kamitsos, L. Wondraczek, Journal of Non-Crystalline Solids. 410, 142 (2015); https://doi.org/10.1016/j.jnoncrysol.2014.11.029

[49] D. Möncke, S. Sirotkin, E. Stavrou, E. I. Kamitsos, L. Wondraczek, D. Möncke, S. Sirotkin, E. Stavrou, Journal of Chemistry and Physics, 141, 224509 (2014); https://doi.org/10.1063/1.4903191

[50] X. Guo, H. Xiao, F. Wang, Y. Zhang, Journal of Physical Chemistry A, 114, 6480 (2010); https://doi.org/10.1021/jp9104147

[51] Y. A. Yamusa, Rosli Hussin, W. N. Wan Shamsuri, S. A. Dalhatu, Aliyu M. Aliyu, Ibrahim Bulus, International Journal of Modern Physics B, 32, 1850213 (2018); https://doi.org/10.1142/S0217979218502132

[52] Mahesh M. Hivrekar, D. B. Sable, M. B. Solunke, K. M. Jadhav, Journal of Non-Crystalline Solids, 474, 58 (2017); https://doi.org/10.1016/j.jnoncrysol.2017.08.028

[53] E. I. Kamitsos, G. D. Chryssikos, Journal of Molecular Structure, 247, 16 pages (1991); https://doi.org/10.1016/0022-2860(91)87058-P

[54] Armenak A. Osipov, Leyla M. Osipova, Journal of Physics and Chemistry Solids, 74, 971 (2013); https://doi.org/10.1016/j.jpcs.2013.02.014

[55] P. Suthanthirakumar, S. Arunkumar, K. Marimuthu, Journal of Luminescence, 202, 289 (2018); https://doi.org/10.1016/j.jlumin.2018.05.069

[56] Mahesh M. Hivrekar, D. B. Sable, M. B. Solunke, K. M. Jadhav, Journal of Non-Crystalline Solids, 491, 14 (2018); https://doi.org/10.1016/j.jnoncrysol.2018.03.051

[57] S. Suresh, P. G. Pavani and V. C. Mouli, Material Research Bulletin, 47, 724 (2012); https://doi.org/10.1016/j.materresbull.2011.12.016

[58] I. I. Kindrat, B. V. Padlyak, R. Lisiecki, V. T. Adamiv, Journal of non-crystalline solids, 521, 119477 (2019); https://doi.org/10.1016/j.jnoncrysol.2019.119477

[59] Cheng Yin, Wu Zhongqing, Hu Xi, Wu Tengyan, Zhou Weiwei, Journal of Rare Earths, 32, 1154 (2014); https://doi.org/10.1016/S1002-0721(14)60138-1

[60] Ki-Soo Lim, P. Babu, C. K. Jayasankar, Sun-kyun Lee, Van-Thai Pham, Hyo-Jin Seo, Journal of Alloys Compound, 385, 12 (2004); https://doi.org/10.1016/j.jallcom.2004.04.133

[61] Y. M Abou Deif, M. M. Algarni, A. M. Emara, H. Algarni, E. S. Yousef, Chalcogenide Letter, 15, 219 (2018).

[62] M. N. Azlan, M. K. Halimah, S. Z. Shafinas, W. M. Daud, Journal of Nanomaterials, 8 pages (2013).